

# Scaling Behavior of Early Stage Dendritic Growth at Low Undercooling

Mathis Plapp and Alain Karma

*Physics Department and Center for Interdisciplinary Research on Complex Systems,  
Northeastern University, Boston, Massachusetts 02115*

(June 23, 1999)

A novel computational method is presented to simulate dendritic growth at realistically low undercooling that combines the phase-field approach with an efficient diffusion Monte Carlo treatment of the large scale diffusion field. It is used to study the formation of the primary dendrite arms in two and three dimensions. With decreasing undercooling, the arm shapes approach self-affine scaling forms with the solidified volume  $\sim t^{d/2}$  and the arm length  $\sim t^{(1+d)/(3+d)}$  in  $d$  dimensions, which correspond to anisotropic Laplacian growth with a diffusion-limited heat flux.

05.70.Ln, 81.30.Fb, 64.70.Dv, 81.10.Aj

The study of dendritic crystal growth has played a central role in shaping our current understanding of how complex interfacial patterns form in non-equilibrium systems governed by relatively simple laws. Although considerable theoretical progress has been made, simulating three-dimensional (3-d) dendritic crystal growth from an undercooled melt for the low undercooling range that corresponds to benchmark experiments [1,2] has remained a major computational challenge. At present, tracking a boundary of complex shape is no longer the main obstacle to simulate dendrites, even in 3-d. This difficulty has been largely overcome by the introduction [3] and subsequent development of the phase-field approach (see Ref. [4] with numerous earlier references therein), which avoids front tracking by smearing the solid-liquid interface over a region of finite width  $W_0$ . Initially, this width was constrained to be comparable to the molecular scale capillary length  $d_0 \sim 10^{-9}$  m, which severely limited quantitative simulations to a range of high undercooling dominated by interface kinetics [5]. By reformulating the asymptotic analysis of the phase-field model, however, it was subsequently made possible to choose this width much larger than  $d_0$ , or about an order of magnitude smaller than the dendrite tip radius  $\rho$ , and to make at the same time kinetic effects arbitrarily small [4]. A daunting difficulty that has remained, however, is the enormous lengthscale gap between  $\rho$  and the several orders of magnitude larger scale of the diffusion field. Progress in coping with this gap has recently been made by using multigrid and adaptive mesh refinement algorithms that make the grid progressively coarser away from the interface [6–8]. Converged quantitative results, however, have so far only been obtained in two dimensions (2-d) [8].

The first goal of this letter is to present a diffusion Monte Carlo (DMC) method that, combined with the phase-field approach, can be used to simulate accurately 3-d dendritic growth for realistically low undercooling. Like adaptive mesh refinement, this method is aimed at closing the gap between  $\rho$  and the large scale diffusion field by solving efficiently the diffusion equation away from the interface and has the important advantage of being relatively simple to implement in both 2-d and 3-d. The second goal is to present results concerning the

early stage of dendritic growth during which four (six) arms in 2-d (3-d) emerge from a structureless nucleus, and then coarsen until reaching steady-state growth after a long transient of duration  $\sim D/v_{ss}^2$ , where  $D$  is the thermal diffusivity and  $v_{ss}$  is the steady-state dendrite tip speed. This transient has been recently studied numerically in 2-d and experimentally under microgravity conditions [9]. In addition, it has been previously studied analytically and numerically [10] as well as experimentally [11] in the context of anisotropic Hele-Shaw Flow that corresponds to 2-d Laplacian growth at constant flux. So far, however, this transient has remained unexplored theoretically in 3-d. Here, we demonstrate numerically and analytically the existence of a 3-d scaling behavior with different exponents than in 2-d. Moreover, we confirm the earlier expectation [10,12] that the 2-d scaling behavior is the same as anisotropic Laplacian growth in the limit of vanishing undercooling, in disagreement with the recent numerical results of Ref. [9].

The solidification of a pure undercooled melt is governed by a well-known set of equations

$$\partial_t u = D \nabla^2 u, \quad (1)$$

$$v_n = D (\partial_n u|_s - \partial_n u|_l), \quad (2)$$

$$u = -d_0 \sum_{i=1}^2 [a(\hat{n}) + \partial_{\theta_i}^2 a(\hat{n})] \kappa_i, \quad (3)$$

where (1) is the diffusion equation in the bulk phases subject to the heat conservation condition (2) and the local equilibrium Gibbs-Thomson condition (3) on the interface. Following common notation,  $u$  is the scaled temperature field that is zero in equilibrium and is equal to  $-\Delta$  in the liquid far from the interface, where  $\Delta$  is the dimensionless undercooling,  $v_n$  is the normal velocity of the interface,  $\theta_i$  are the local angles between the normal  $\hat{n}$  to the interface and the two local principal directions on the interface,  $\kappa_i$  are the principal curvatures, and  $a(\hat{n}) \equiv (1 - 3\epsilon_4)[1 - 4\epsilon_4/(1 - 3\epsilon_4)(n_x^4 + n_y^4 + n_z^4)]$  is the anisotropy function for a cubic crystal.

The basic idea of our method is to divide space into an ‘inner’ and an ‘outer’ domain as illustrated in Fig. 1. The inner domain consists of the growing structure and a

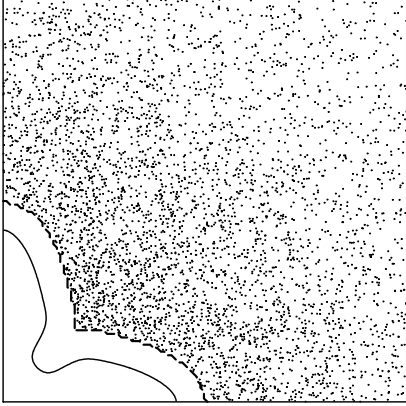


FIG. 1. Snapshot of a 2-d simulation for  $\Delta = 0.1$  and  $\epsilon_4 = 0.025$ : solid-liquid interface (solid line), inner-outer domain boundary (dashed-line), and random walkers (dots). Only a small part of the outer domain and one out of 50 walkers are shown for clarity.

thin ‘buffer layer’ of liquid surrounding the interface. The outer domain corresponds to the rest of the liquid, and is much larger than the inner domain at low undercooling. In the inner domain, we integrate the standard *deterministic* phase-field equations using the method exposed at length in Ref. [4], although our DMC method is also compatible with other front tracking methods. In contrast, in the outer domain, the diffusion equation is simulated *stochastically* by an ensemble of *off-lattice* random walkers. Walkers are created and absorbed at the boundary between inner and outer domain at a rate which is proportional to the local heat flux. The temperature in the outer domain is related to the local density of walkers, and the boundary conditions for the integration in the inner region are obtained by averaging this density over coarse-grained boxes near to the boundary.

The idea of solving the diffusion or Laplace equation with an ensemble of random walkers is well-known and has been used previously to simulate diffusion-limited growth [13] and Hele-Shaw flow [14]. The main new feature of our method, however, is that we have separated the solid-liquid interface from the boundary at which the conversion from the deterministic to the stochastic solution of the diffusion equation takes place. This separation yields two essential benefits. Firstly, it makes it possible to use the phase-field approach with its proven accuracy to simulate the interface evolution and to resolve even a weak crystalline anisotropy, without being affected by the details of the conversion process. Secondly, in the buffer layer between the solid-liquid interface and the conversion boundary, the temperature obeys the deterministic diffusion equation. Consequently, the noise created by the stochastic release and impingement

of walkers is rapidly damped away from the conversion boundary. Hence, the amplitude of temperature fluctuations at the *solid-liquid interface* can be reduced to an insignificant level without much cost in computation time by increasing the thickness of the buffer layer.

In the outer region, each walker is represented by a set of variables indicating its position and the time it has next to be updated. To update a walker, a new position is randomly selected with a probability distribution given by the diffusion kernel,

$$P(\vec{x}', t' | \vec{x}, t) = \frac{1}{[4\pi D(t' - t)]^{d/2}} \exp -\frac{|\vec{x}' - \vec{x}|^2}{4D(t' - t)}, \quad (4)$$

where  $\vec{x}$  and  $\vec{x}'$  are the old and new positions of the walker, respectively, and  $t' - t$  is the time increment between updates. This representation of the diffusion equation is widely used in quantum Monte Carlo methods [15]. The key improvement that makes the algorithm efficient in the present context is the introduction of a variable step size: we allow walkers to take progressively larger steps with increasing distance away from the interface, and to be concomitantly updated more rarely, which does not affect the quality of the solution near the solid-liquid interface. Typically, we vary the average step size between a value comparable to the spacing of the inner mesh to about 100 times that value. Our test computations show that the far field can be evolved at essentially no extra cost: the program spends most of its time in the inner region and for the walkers which are near to the conversion boundary and have to make small steps. Thus this ‘adaptive step’ implementation yields essentially the same benefits as an adaptive meshing algorithm, while avoiding the overhead of regridding. Moreover, our method can be easily parallelized as demonstrated in the simulation of Fig. 2 that took about 6 hours on 64 processors of the CRAY T3E at NERSC and used  $5 \times 10^6$  walkers at the end of the run. A more detailed exposition of our method including benchmark comparisons with deterministic phase-field simulations will be presented elsewhere.

To study growth transients, we started our simulations from a small spherical solid nucleus with a uniformly undercooled temperature  $u = -\Delta$  and exploited the cubic symmetry to reduce simulation time. We recorded the arm length  $L(t)$ , the tip velocity  $v(t) = \dot{L}(t)$ , the tip radius of curvature  $\rho(t)$ , and the total volume of solid  $V_s(t)$ . The value  $\epsilon_4 = 0.025$  that corresponds to the experimentally estimated anisotropy value for pivalic acid (PVA) [16] was used in all the simulations reported here.

Let us now examine how the scaling behavior of 2-d and 3-d transients can both be understood within a unified picture of diffusion limited anisotropic Laplacian growth. In the limit  $\Delta \rightarrow 0$ , the diffusion field surrounding the arms grows initially  $\sim (Dt)^{1/2}$ , and thus much faster than  $L(t)$  since the tip velocity vanishes in this limit. Therefore,  $u$  can be assumed to obey Laplace’s equation on the scale of  $L(t)$  subject to the boundary

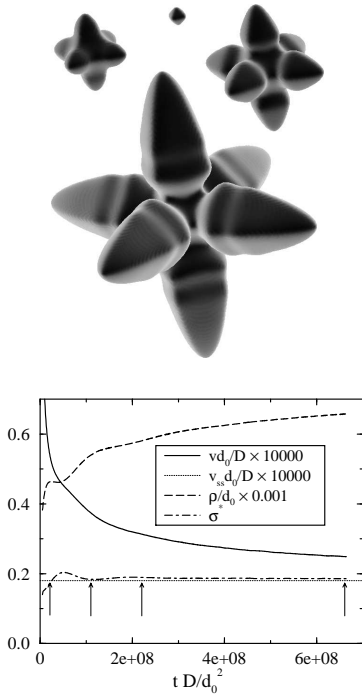


FIG. 2. Scaled tip velocity, tip radius, and  $\sigma^*$  vs time for  $\Delta = 0.05$  and  $\epsilon_4 = 0.025$  with (top) snapshots of the 3-d structure at the times corresponding to the arrows. The final arm length is  $145 \mu\text{m}$  after  $0.14 \text{ s}$  for  $D$  and  $d_0$  of PVA [2] and  $290 \mu\text{m}$  after  $15 \text{ s}$  in the run at  $\Delta = 0.01$  of Fig. 4b.

conditions (2) and (3) on the interface. On the other hand, the far field on the scale  $(Dt)^{1/2}$ , which obeys the full diffusion equation, sets the total heat flux  $F$  that arrives at the dendrite, which can be determined from the self-similarity solution of a growing  $d$ -dimensional sphere. This solution is well-known and yields  $F = 4\pi p_d D (16p_d Dt)^{(d-2)/2}$  where the  $d$ -dimensional Peclet number  $p_d(\Delta)$  is implicitly defined for  $d = 2, 3$  by

$$\Delta = p_d^{d/2} \exp(p_d) \int_{p_d}^{\infty} y^{-d/2} e^{-y} dy. \quad (5)$$

Heat conservation imposes  $\dot{V} = F$ , which yields that the volume of solid grows linearly in time in 2-d,  $V_s = 4\pi p_2 Dt$ , and as  $V_s = (4\pi/3)(4p_3 Dt)^{3/2}$  in 3-d.

Next, to describe the arm evolution, one needs to solve the anisotropic Laplacian growth problem with the boundary condition  $\partial_r u = -F/[D\pi(2r)^{d-1}]$  for  $r \gg L$ . In 2-d,  $F$  is constant and this problem is precisely the problem of anisotropic Hele-Shaw flow studied analytically by Almgren, Dai, and Hakim [10]. One minor difference is that there is no flux in the solid in the Hele-Shaw flow analog of Eq. 2, but this can be accounted for in the tip solvability condition. By solving Laplace's equation on the scale of  $L(t)$  using conformal mapping and by imposing a solvability condition at the tip, these authors obtained that the shape of an arm growing along  $x$  follows a self-affine evolution  $y(x, t) = t^\beta \tilde{y}(x/t^\alpha)$  with

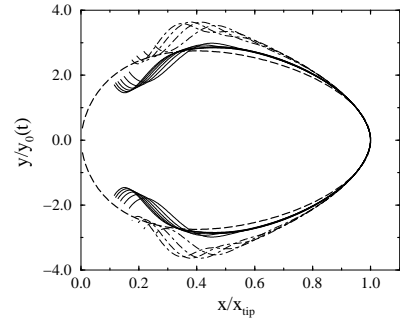


FIG. 3. Superimposed dendrite arm shapes scaled in  $x$  and  $y$  by  $x_{tip} = L(t)$  and  $y_0(t) = y(0.95 x_{tip})$  for  $\Delta = 0.05$  and  $\epsilon_4 = 0.025$ . Solid lines: 2-d, dash-dotted lines: sections of 3-d shapes in a (100) plane. Times range from  $21.5 t_0$  to  $60 t_0$  in 2-d and  $6 t_0$  to  $12 t_0$  in 3-d with  $t_0$  defined in the caption of Fig. 4. Dashed line: theoretical scaling shape for 2-d anisotropic Laplacian growth rescaled as described above.

the exponents  $\alpha = 3/5$  and  $\beta = 2/5$ , where  $y$  is the coordinate perpendicular to the growth direction.

In 3-d, the anisotropic Laplacian growth problem with a time-dependent flux  $F \sim t^{1/2}$  has no known analytical solution on the scale of  $L(t)$ . We will assume the existence of an axisymmetric scaling solution in 3-d of the same form as in 2-d, with  $y$  being the coordinate perpendicular to the growth axis. Although Fig. 2 clearly shows that the dendrite arms are not axisymmetric bodies of revolution, our simulation results demonstrate that this approximation is fairly accurate and captures the dominant behavior. Next, we note that the scaling exponents can be determined from the time dependence of the volume  $V_s \sim t^\nu$  obtained from the diffusive similarity solution,  $\nu = d/2$ , and the solvability condition imposed at the tip, *without* needing to calculate explicitly the self-similar shape  $\tilde{y}$ . The former yields a first condition  $\alpha + (d-1)\beta = \nu$ . The tip solvability condition states that  $\sigma^* = 2d_0 D / [\rho^2(t)v(t)]$  is constant as soon as tips are formed, as illustrated in 3-d in Fig. 2. Physically, this is a direct consequence of the fact that  $v(t)$  and  $\rho(t)$  evolve slowly on the tip diffusion time scale  $\rho^2/D$  where  $\sigma^*$  is established. This yields at once the second condition  $4\beta - \alpha - 1 = 0$ , and thus combined with the first,  $\alpha = (1+d)/(3+d)$  and  $\beta = (2+d)/(6+2d)$ , or  $\alpha = 2/3$  and  $\beta = 5/12$  in 3-d.

Our numerical results are in good quantitative agreement with these predictions in 2-d and 3-d. The solid volume grows slightly more rapidly than predicted by the self-similarity solution, but for the smallest  $\Delta$  values simulated in 2-d and 3-d, the volumes of the well-developed final dendrites exceed by only 20% these predictions. The arm shapes nicely scale in both 2-d and 3-d (Fig. 3). In 2-d, the shape agrees reasonably well with the analytically predicted shape for Laplacian growth [10]. The good superposition of the curves even far from the tip indicates that a large part of the structure scales

as the tip region. In Fig. 4, we plot the functions  $\alpha(t) = d(\ln L)/d(\ln t)$  and  $\nu(t) = d(\ln V_s)/d(\ln t)$ , which allows us to observe the cross-over from the early stage scaling behavior towards steady-state growth ( $\alpha = 1$ ). In both dimensions  $\alpha(t)$  and  $\nu(t)$  become increasingly flatter with decreasing  $\Delta$ , as expected, and approach the analytically predicted exponents. Finite diffusive corrections to the analytical predictions are reflected in a slow rise of  $\alpha(t)$  and  $\nu(t)$ . These corrections originate from the fact that the diffusion equation can only be approximated by Laplace's equation on the scale of the dendrite in the limit  $L(t)/(Dt)^{1/2} \rightarrow 0$ , whereas this ratio is finite and increases with time in our simulations. Although they vanish in the limit  $\Delta \rightarrow 0$ , these corrections are larger in 3-d than in 2-d at the same  $\Delta$  (Fig. 4) because of the well-known fact that the tip velocities are larger in 3-d than in 2-d. Thus, we observe convergence to the theoretically expected Laplacian scaling in this limit, in disagreement with the conclusions of Provatas *et al.* in [9]. In particular, for  $\Delta = 0.05$  and  $\epsilon_4 = 0.025$ , these authors reported a 2-d exponent  $\alpha = 0.73$ , whereas for the same parameters our curve  $\alpha(t)$  in Fig. 4(a) remains close to  $\alpha = 3/5$  for more than a decade in time.

To conclude, we remark that two conditions must be met for the 3-d scaling behavior to be experimentally observable. Firstly, the effect of interfacial kinetics, which has been neglected here, must be sufficiently small for  $\sigma^*$  to remain constant during the duration of the transient, which is still an open question for PVA. Secondly, the undercooling must be small enough for the duration of a pure scaling transient, i.e. characterized by a single *time-independent* exponent, to be on an experimentally observable time scale. The results reported in Fig. 4b used in conjunction with the thermophysical data of PVA [2] indicate that this duration is  $\sim 0.1$  s at  $\Delta = 0.05$ , but larger than  $\sim 10$  s at  $\Delta = 0.01$ . For materials with lower anisotropy such as succinonitrile, scaling transients should last considerably longer at the same undercooling. Finally, we do not expect that the scaling behavior is significantly affected by the presence of noise-driven side-branches. This question, however, could be addressed using the present method with the addition of thermal noise into the phase-field equations [17].

This research is supported by U.S. DOE Grant No. DE-FG02-92ER45471 and benefited from computer time allocation at NERSC and NU-ASCC. We thank Flavio Fenton for help with 3-d visualization of our simulations and Vincent Hakim for fruitful conversations.

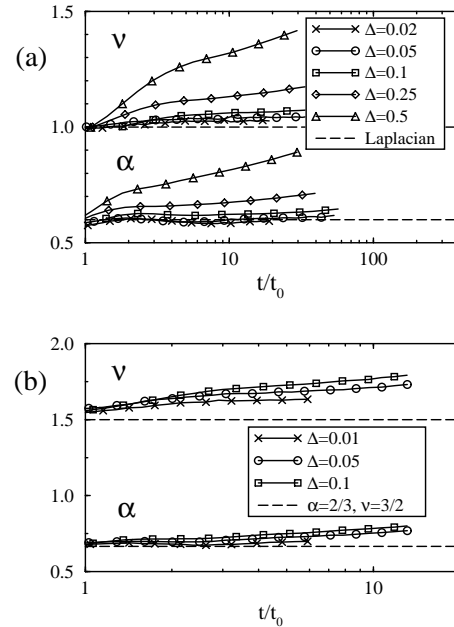


FIG. 4. Functions  $\alpha(t)$  and  $\nu(t)$  vs scaled time  $t/t_0(\Delta)$  in 2-d (a) and 3-d (b). In order to show all curves on the same plot,  $t_0(\Delta)$  was defined to be the time at which the tips are ahead of the grooves by about two tip radii. In order of decreasing  $\Delta$ ,  $t_0 D/d_0^2 = 2.29 \times 10^4$ ,  $9.03 \times 10^5$ ,  $4.36 \times 10^7$ ,  $5.35 \times 10^8$ , and  $1.39 \times 10^{10}$  in 2-d, and  $4.18 \times 10^6$ ,  $5.58 \times 10^7$  and,  $1.17 \times 10^{10}$  in 3-d.

Growth **112**, 84 (1991).

- [3] J. S. Langer, in *Directions in Condensed Matter*, ed. by G. Grinstein and G. Mazenko (World Scientific, Singapore, 1986), p. 164; J. B. Collins and H. Levine, Phys. Rev. B **31**, 6119 (1985).
- [4] A. Karma and W.-J. Rappel, Phys. Rev. E **57**, 4323 (1998).
- [5] S.-L. Wang and R. F. Sekerka, Phys. Rev. E **53**, 3760 (1996).
- [6] A. Schmidt, J. Comput. Phys. **125**, 293-312 (1996).
- [7] R. J. Braun and M. T. Murray, J. Cryst. Growth **174**, 41 (1997).
- [8] N. Provatas, N. Goldenfeld, and J. Dantzig, Phys. Rev. Lett. **80**, 3308 (1998).
- [9] N. Provatas *et al.*, Phys. Rev. Lett. **82**, 4496 (1999).
- [10] R. Almgren, W.-S. Dai, and V. Hakim, Phys. Rev. Lett. **71**, 3461 (1993).
- [11] J. Ignés-Mullol and J. Maher, Phys. Rev. E **53**, 3788 (1996).
- [12] E. Brener, Phys. Rev. Lett. **71**, 3653 (1993).
- [13] T. Vicsek, Phys. Rev. Lett. **53**, 2281 (1984).
- [14] L. P. Kadanoff, J. Stat. Phys. **39**, 267 (1985); S. Liang, Phys. Rev. A **33**, 2663 (1986).
- [15] See for example S. E. Koonin and D. C. Meredith, *Computational Physics* (Addison-Wesley, Redwood City, 1992).
- [16] M. Muschol, D. Liu, and H. Z. Cummins, Phys. Rev. A **46**, 1038 (1992).
- [17] A. Karma and W.-J. Rappel, Phys. Rev. E, in press.

[1] S.-C. Huang and M. E. Glicksmann, Acta Metall. **29**, 701 (1981); U. Bisang and J. Bilgram, Phys. Rev. Lett. **75**, 3898 (1995).

[2] E. R. Rubinstein and M. E. Glicksmann, J. Cryst.